# The effect of adsorbed oxygen species on carbon-resistance of Ni-Zr catalyst modified by Al and Mn for dry reforming of methane

Ye Wang, Li Li, Patrick Da. Costa, Changwei Hu, Chaojun Cui

# The effect of adsorbed oxygen species on carbon-resistance of Ni-Zr catalyst modified by Al and Mn for dry reforming of methane

**Ye Wang [a, b], Li Li [c], Chaojun Cui [a], Patrick Da. Costa [b, *] and Changwei Hu [a, c, *]**

a: College of Chemical Engineering, Sichuan University, Chengdu, Sichuan 610065, P. R. China

b: Sorbonne Université, Institut Jean Le Rond d'Alembert, CNRS, 2 Place de la Gare de Ceinture, Saint-Cyr-L'Ecole 78210, France

c: Key Laboratory of Green Chemistry and Technology, Ministry of Education, College of Chemistry, Sichuan University, Chengdu, Sichuan, 610064, P. R. China

E-mail: patrick.da_costa@upmc.fr (P. Da Costa) and changweihu@scu.edu.cn. (C. Hu)

**Abstract:**

Dry reforming of methane was investigated over Ni-Zr catalysts modified by Aluminum and Manganese. The catalysts were characterized by XRD, $CO_2$-TPD, XPS, TGA, and Raman. Among all prepared catalysts, the 5Al-5Mn (5 wt% Al and 5 wt% Mn) catalyst showed the highest $CH_4$ and $CO_2$ conversion at 700 $^oC$ DRM with low carbon deposition. The $CO_2$-TPD results exhibited that the 5Al-5Mn catalyst had the highest amounts of both total basic sites and medium-strength basic sites, which could promote the adsorption and activation of $CO_2$ molecule during the DRM reaction, and further reduce the carbon deposition. The XRD results suggested that the addition of both Al and Mn led to smaller nickel particle size. Besides, the lower carbon deposition on 5Al-5Mn and 2.5Al-7.5Mn catalyst was derived from a higher content of surface adsorption oxygen species, which was verified by the O 1s results. While the lower number of basic sites, more strong basic sites and larger particle size on 5Mn and 5Al catalysts result in a higher amount of carbon deposition.

**Keywords:** Carbon resistance, Dry reforming of methane, Adsorbed oxygen species, Manganese, Aluminum

## 1. Introduction

Nowadays, there is a huge interest in topics focusing on alternative energy, global warming, and greenhouse gases. Because the limited oil reserves decrease rapidly, other renewable sources need to be exploited [1]. Dry reforming of methane (DRM) offers an interesting opportunity to address these problems since it can utilize marsh gas and biomass pyrolysis gas directly [2, 3]. The nickel is the most appropriate catalyst for DRM due to high activity and low-cost [4-6]. However, Ni-based catalysts are suffered from deactivation through the sintering of metal and carbon deposition [4, 7]. So, a lot of studies have been investigated in the carbon-resistant for DRM [8-14].

Generally, promoters are used in order to reduce the carbon deposition over nickel-based catalyst via the following mechanisms: i) promoters could increase the number of basic sites, which could promote the adsorption and/or activation of $CO_2$; ii) promoters could enhance the dispersion of nickel particles; iii) promoters could promote the formation of oxygen vacancies [15-21]. Pompeo [22] investigated the influence of α-$Al_2O_3$, $ZrO_2$, and α-$Al_2O_3$-$ZrO_2$ on the performance of catalysts. The author found that Ni/α-$Al_2O_3$-$ZrO_2$ showed higher stability for 700 $^oC$ DRM reaction, due to the lower coke formation on Ni/α-$Al_2O_3$-$ZrO_2$ catalyst; because both $Al_2O_3$ and $ZrO_2$ could increase the $CO_2$ adsorption and further decrease the carbon deposition. Wang et al. [23] studied Mn doping nanocrystalline Co–Ce–Zr–$O_x$ catalysts for DRM reaction. The conversions of $CO_2$ and $CH_4$ were 74 % and 70 %, respectively. While the conversions of $CO_2$ and $CH_4$ were both lower than 40 % on non-promoted nanocrystalline Co–Ce–Zr–$O_x$ catalyst. The promoted activity was attributed to the increasing availability of surface oxygen species and the better oxygen mobility on Mn-modified catalyst, as well as the better dispersed nano-sized $Co_3O_4$. Bellido et al. [24] prepared nickel supported on $ZrO_2$ stabilized with various content of $Y_2O_3$. The Ni/8$Y_2O_3$–$ZrO_2$ (with a $Y_2O_3$ load of 8 mol%) catalyst showed the best catalytic performance for DRM reaction with the initial $CH_4$ conversions of 72 %. The author found the interaction between the surface oxygen vacancies and nickel species on the $Y_2O_3$–$ZrO_2$ support enhanced by the increasing $Y_2O_3$ load, which could improve the $CH_4$ and $CO_2$ conversion in the dry reforming of methane reaction. Besides, according to the literature [15, 20], the surface oxygen vacancies could promote the elimination of coke, because the surface oxygen vacancies could induce oxygen radicals from the $CO_2$ to react with carbon deposition.

The promotion of Al resulted in higher activity for DRM due to the higher reducibility and dispersion of nickel, reported by Liu et al. [25]. Talkhoncheh et al. [26] analyzed the effect of clinoptilolite, ceria, and alumina supports on the activity for DRM. The $Ni/Al_2O_3$ catalyst exhibited the highest catalytic performance since the even distributions and high specific surface area. The addition of Mn can contribute to carbon removal with the sacrifice on the activity [27]. Yao et al. [28] and Seok et al. [29] also found that Mn promoter could reduce the carbon deposition by the smaller particle size of nickel species. The introduction of Al and Mn was conducive to the activation for DRM, reported by Li et al. [30].

Herein, we prepared Ni-Zr materials promoted by Mn and Al, which were applied to the dry reforming of methane. To understand the relationship between the carbon deposition and the surface structure of the catalysts, $CO_2$-TPD, XRD, XPS, TGA, and Raman were conducted.

## 2. Experiment

### 2.1 The preparation of catalysts

The catalysts are prepared via a one-step synthesis method route [31]. P123, $Ni(NO_3)_2{\cdot}6H_2O$, $ZrO(NO_3)_2{\cdot}xH_2O$, $CH_4N_2O$, and $Al(NO_3)_3{\cdot}9H_2O$ and/or $Mn(NO_3)_2{\cdot}4H_2O$ were dissolved in distilled water (375 mL). The molar loadings of Ni, Al, Zr, and Mn were listed in **Table 1**. The mixture of aqueous solutions was heated from room temperature to 95 °C under vigorous stirring for 48 h in air. Then this suspension was subsequently aged in an oven (100 °C) for 24 h in a closed vessel. Next, this slurry was suction filtered and washed by distilled water with equal volume of obtained materials for three times. The solids obtained were dried at room temperature. Finally, the precursor was calcined at 800 °C for 5 h with an increasing rate of 1 °C/min under airflow. The catalysts were denoted as 5Al, 7.5Al–2.5Mn, 5Al–5Mn, 2.5Al–7.5Mn, and 5Mn respectively.

**Table 1** The molar loadings of Ni, Zr, Al, and Mn on a series of promoted Ni-Zr materials

| Catalyst | Nickel % | Zirconium % | Aluminum % | Manganese % |
|---|---|---|---|---|
| 5Al | 10 | 85 | 5 | - |
| 7.5Al–2.5Mn | 10 | 80 | 7.5 | 2.5 |
| 5Al–5Mn | 10 | 80 | 5 | 5 |

| | | | | |
|---|---|---|---|---|
| 2.5Al–7.5Mn | 10 | 80 | 2.5 | 7.5 |
| 5Mn | 10 | 85 | - | 5 |

### 2.2 The catalytic performance of catalysts

The DRM activity test was performed in a fixed-bed flow microreactor with a K-type thermocouple to monitor the temperature of the catalytic bed. At first, the catalysts were reduced at 750 °C under the 5 vol% $H_2$/Ar flow for one hour. And then, the surface of reduced catalysts was cleaned by argon flow. Last, the mixed gases were introduced to the catalyst bed. The ratio of $CO_2$: $CH_4$: Ar was 1: 1: 8, corresponding to a GHSV of 48,000 $h^{-1}$. The effluents were analyzed by using an online gas micro chromatography (490 Varian Micro-GC). The $H_2$/CO molar ratio and the conversions of $CH_4$ ($X_{CH_4}$) and $CO_2$ ($X_{CO_2}$) and were calculated as follows:

$$X_{CH_4} = \frac{n_{CH_4,in} - n_{CH_4,out}}{n_{CH_4,in}} \times 100\% \quad (1)$$

$$X_{CO_2} = \frac{n_{CO_2,in} - n_{CO_2,out}}{n_{CO_2,in}} \times 100\% \quad (2)$$

$$H_2/CO = n_{H_2,out}/n_{CO,out} \quad (3)$$

Where $X_i$ and $H_2/CO$ refers to the conversion of $i$ species, and the molar ratio of $H_2$/CO. The $n_{j,in}$ is the number of moles of $j$ species in feed gas. The $n_{j,in}$ is the number of moles of $j$ species in out gas.

### 2.3 The characterization of catalysts

The $CO_2$-TPD experiments in the range of 80 to 900 °C were measured on a BELCAT-M measurement, equipped with a TCD. The fixed-bed reactor loaded with ca. 60 mg of sample, using a heating rate of 10 °C/min. After an *in-situ* reduction at 750 °C under a 5 % $H_2$/Ar flow, the sample was cooled down to 80 °C, introducing in a mixture flow of 10% $CO_2$/He for 60 min. Last, the desorption process was under a He flows with an increasing temperature (80 to 900 °C).

The powder XRD patterns were recorded on a DX-1000 CSC diffractometer with a Cu Kα radiation source. The voltage and current were 40 kV and 25 mA, respectively. The Bragg angles were recorded in the range of 10 ° < 2θ < 80 °, with 0.3 s $step^{-1}$ scan speed and 0.03 ° scan step size. The crystallite size on catalysts was calculated by using the Scherrer Equation.

The thermogravimetric analysis (TGA) was conducted on the NETZSCH STA 449F5 instrument.

The temperature of the sample was increased from 35 to 800 °C with a heating rate of 5 °C/min, and at the same time, the sample was oxidized by air flow (60 ml/min). The weight of the sample was recorded from 35 to 800 °C.

The X-ray photoelectron spectroscopy (XPS) was conducted on a KRATOS spectrometer with an AXIS Ultra DLD to detect the surface elements of catalysts.

Raman spectroscopy experiments were conducted on an objective (X50LWD) with a Grating of 600 gr/mm, a Laser of 532.17 nm, a Hole of 200 μm, and a Filter of D1. The data was collected from the wavenumber values of 1000−2000 $cm^{-1}$.

## 3. The results and discussion

3.1 Catalytic activity for $CO_2$ reforming of methane at medium temperature

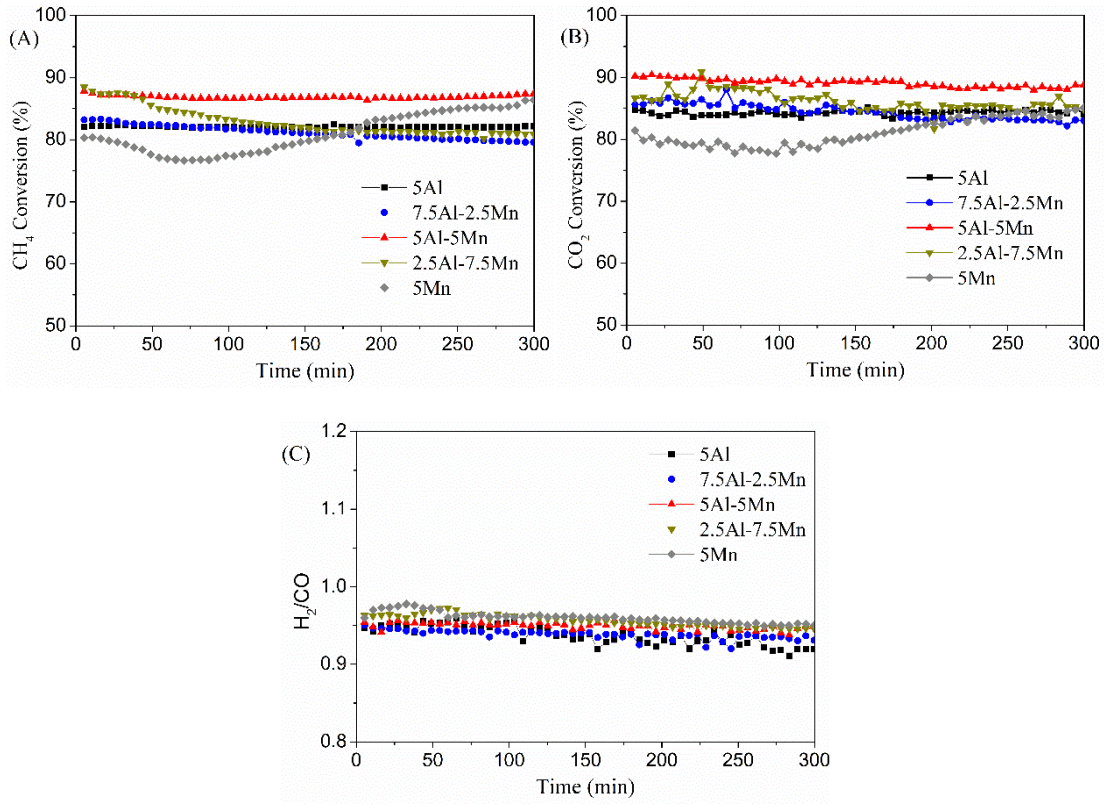


**Figure 1** The conversion of $CH_4$ (A) and $CO_2$ (B), and (C) the rate of $H_2$/CO of the series of Al-Mn-Ni-Zr catalysts at 700 $^oC$.

The effect of Al and/or Mn promoters was investigated in previous work [25, 28, 32, 33]. It was shown that the catalytic performance of Al-promoted catalysts was higher than that of non-promoted catalyst. Liu et al. [25] and He et al. [33] reported the introduction of Al results in

low Ni particle sizes, thereby enhancing the activity for DRM. The references [25, 28] reported that the Mn promoter could enhance the carbon-resistance of nickel-based catalysts with a decrease of catalytic activity. The Ni-Zr catalyst exhibited a decrease activity within 100 min, which was lower than 5Al-5Mn catalyst (Figure S1). Herein, the two promoters Al and Mn were combined for designing a novel type of Al-Mn promoted Ni-Zr catalyst to obtain a higher catalytic performance for DRM.

Ni-Zr catalysts modified by the various ratio of Al/Mn promoters were tested in DRM at 700 $^{o}$C with GSHV of 48,000 $h^{-1}$, for 300 minutes of time-on-stream (TOS) with the mixed flow of $CH_4$: $CO_2$: Ar=1: 1: 8. The results of activity tests are presented in **Figure 1**, including both conversions of $CH_4$ and $CO_2$, and the molar ratio of $H_2$/CO for a series of Ni-Zr catalysts. All the series of Ni-Zr catalysts were found to be catalytically active for both $CO_2$ and $CH_4$ conversions (> 80 %) for the initial reaction time-on-stream. As given in **Table 2**, the initial methane conversion was 82.0 %, 83.2 %, 87.8 %, 88.5 % and 80.3 % respectively for 5Al, 7.5Al-2.5Mn, 5Al-5Mn, 2.5Al-7.5Mn and 5Mn. The $CO_2$ conversion followed the sequence: 90.2 for 5Al-5Mn > 86.6 % for 2.5Al-7.5Mn > 85.6 % for 7.5Al-2.5Mn > 83.8 % for 5Al > 81.4 for 5Mn. However, a little bit of difference appeared when the activity of the Ni-Zr catalysts was compared with time on stream. The $CH_4$ conversion increased with TOS on the 5Mn catalyst. A similar observation of increased activity was reported by Li et al. [34]. The author found that Mn improved the dispersion of nickel species and enhanced the interaction between nickel and support with TOS, and further enhanced the catalytic for DRM. While the $CH_4$ conversion decreased on other catalysts, especially on 2.5Al-7.5Mn, it decreased by 8.6 %. The relative changes in $CH_4$ conversion were not significant for the 5Al-5Mn catalyst, manifesting this was the most stable catalytic activity among the studied catalysts. A similar trend can be observed for the relative change in $CO_2$ conversion, i.e. -0.8, -3.9, -1.6, -2.0, and +4.8 for 5Al, 7.5Al-2.5Mn, 5Al-5Mn, 2.5Al-7.5Mn, and 5Mn catalysts, respectively.

**Table 2** The initial and after 5h activity, and the relative change in activity.

| | Initial conversion | | 5 h conversion | | Δ: Relative change after 5 h | |
|---|---|---|---|---|---|---|
| Catalysts | $CH_4$ (%) | $CO_2$ (%) | $CH_4$ (%) | $CO_2$ (%) | $CH_4$ (%) | $CO_2$ (%) |
| 5Al | 82.0 | 84.7 | 81.0 | 84.0 | -1.2 | -0.8 |

| | | | | | | |
|---|---|---|---|---|---|---|
| 7.5Al-2.5Mn | 83.2 | 85.6 | 79.5 | 82.3 | -4.5 | -3.9 |
| 5Al-5Mn | 87.8 | 90.2 | 87.4 | 88.7 | -0.4 | -1.6 |
| 2.5Al-7.5Mn | 88.5 | 86.6 | 80.9 | 84.9 | -8.6 | -2.0 |
| 5Mn | 80.3 | 81.4 | 86.5 | 85.3 | +7.7 | +4.8 |

Besides, the 5Mn catalyst presents the highest ratio of $H_2$/CO than the studied catalysts, as presented in **Figure 1** (C). The ranking in $H_2$/CO ratio is found as follows: 5Mn > 5Al-5Mn > 2.5Al-7.5Mn > 7.5Al-2.5Mn > 5Al. Side reactions such as the reverse water-shift reaction (RWGS) and the disproportionation of CO reaction could results in the lower than unity $H_2$/CO ratio [15, 20, 35]. The disproportionation of CO reaction ($2CO \rightarrow CO_2 + C$, $\Delta H = -172.4\,kJ/mol$) is a highly exothermic reaction [36]. Thermodynamically, the reaction is favoured at low temperatures and high pressure. Besides, the RWGS reaction is thermodynamically favorable and rapid to reach equilibrium under the reaction temperature between 500 and 700 °C [37, 38]. Thus, both RWGS and the disproportionation of CO could give rise to the lower $H_2$/CO ratio at 700 °C. Besides, the $CO_2$ conversion is higher than the $CH_4$ conversion on all the catalysts. Meanwhile, the ratio of $H_2$/CO shows a decreasing trend on 5Al, 7.5Al-2.5Mn, 2.5Al-7.5Mn, and 5Mn catalysts, suggesting that the reverse water-shift reaction is promoted with TOS [30]. In the whole process, the 5Al-5Mn catalyst exhibited the highest activity and stability in the 5 h time on stream for dry reforming of methane.

3.2 Carbon deposition analysis

According to the literature, the promotion by Mn could lead to a decrease in the carbon deposition of Ni-based catalysts during the DRM reaction [25, 28, 29, 39]. Herein, the carbon deposition on spent catalysts was measured by TGA experiments (**Figure 2**). It is worth noting that a small weight increase is observed in the 200-400 $^oC$ range on all the catalysts, which is consistent with our previous work [31, 40], and resulted from $Ni^0$ oxidation to NiO. Then a weight decline is observed at 400-700 $^oC$ and arises from the removal of different types of carbon species. Thus, the carbon deposition on spend catalysts was 2.5 %, 3.6 %, 6.3 %, 11.1 % and 14.0 % on 2.5Al-7.5Mn, 5Al-5Mn, 5Mn, 7.5Al-2.5Mn and 5Al catalysts, respectively. Both Al and Mn promoted catalysts

exhibited lower carbon deposition, indicating that the promotion of both Al and Mn could reduce the carbon deposition in DRM. The 2.5Al-7.5Mn catalyst exhibited the lowest carbon deposition since the conversion of $CH_4$ decreases with time on stream, while the $CO_2$ conversion does not change. Thus, the higher $CO_2$ conversion related to parallel reactions taking place during the DRM reaction, which can promote carbon removal during DRM. Besides, the 7.5Al-2.5Mn catalyst displays behavior different from other catalysts containing Al. The decrease in weight starts at around 350 $^{o}$C in comparison to other catalysts in which the start is around 450°C. Meanwhile, two peaks in the DSC curve can be observed at 350-700 $^{o}$C on the 7.5Al-2.5Mn catalyst. All the DSC signals imply that both processes (the oxidation of $Ni^0$ species and the elimination of carbon species) have an exothermic character, which has been reported in the literature [40]. The best results for both activity and carbon deposition were obtained for the 5Al-5Mn catalyst.

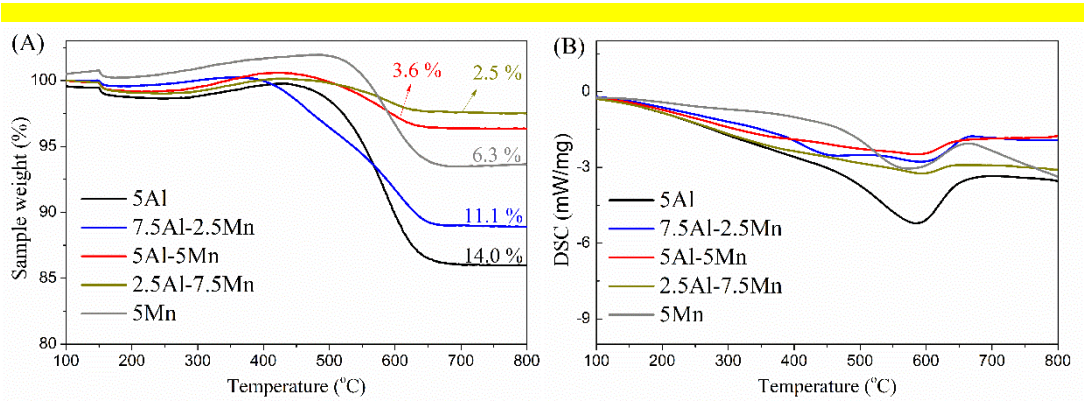


**Figure 2** The TGA profiles of a series of used Al-Mn-Ni-Zr catalysts, (A) The sample weight curve and (B) the DSC curve.

In order to define the carbon species formed during DRM on the studied catalysts, Raman spectroscopy was performed. The results are reported in **Figure 3**. Two peaks at about 1350 and 1580 $cm^{-1}$ could be observed on all spent Ni-Zr-Al-Mn catalysts, which can be assigned to the D band (from disorder) and G band (from graphite), respectively, as reported elsewhere [35, 41, 42]. The intensity of D ($I_D$) and G ($I_G$) band on both 5 Al-5Mn and 2.5Al-7.5Mn catalysts is weaker than that on others, which is in agreement with the TAG analyses. The D band results from the defective graphite unit cell, which is broken by an edge atom or a heteroatom [43]. The $I_D$ and $I_G$ are the peak area of D and G band in the curve of Raman, respectively. And the ratio of $I_D/I_G$ is related to the parameter of defectiveness of carbon materials [44]. After 5 h (300 min) of the DRM

test, the 7.5Al-2.5Mn catalyst exhibits the highest $I_D/I_G$ (1.0), others are 0.9, 0.8, 0.7, 0.5 for 5Al, 5Al-5Mn, 2.5Al-7.5Mn and 5Mn catalysts, respectively. These later results imply that the addition of Mn can decrease the ratio of $I_D/I_G$. According to the literature [28, 29], the addition of Mn as promoter can reduce the carbon deposition over Ni-based catalysts due to the smaller nickel particle size. Herein, the lower $I_D/I_G$ ratio manifests that manganese also can promote the formation of graphite.

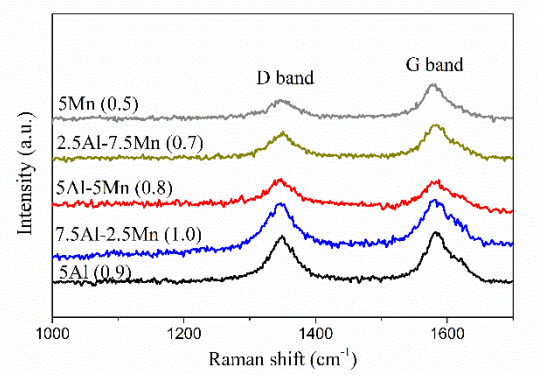


**Figure 3** The Raman profiles of used Al-Mn-Ni-Zr catalysts

Besides, concerning the types of carbon deposition on 5Al and 5Mn catalysts. The decrease in weight over 5Al catalyst starts at around 450 °C (**Figure 2**), while it shifts to 530 $^{o}$C on 5Mn catalyst, which might mean different types of carbon on 5Al and 5Mn catalyst. Besides, the DSC curve of 5Al catalyst exhibited a wide peak at 200 to 450 $^{o}$C and a main peak at about 580 $^{o}$C. Whereas for 5Mn catalyst, the DCS curve showed a very weak and wide peak at 350 to 450 $^{o}$C and a main peak at 580 $^{o}$C. According to the Raman results, the ratio of $I_D/I_G$ is 0.9 and 0.5 on 5Al and 5Mn catalysts, respectively, indicating that more content of D band carbon formed on 5Al catalyst. In our previous work [35]. The D band carbon was easy to be removed. Thus, the carbon with higher content of D band on 5 Al catalyst was easy to be removed. Besides, this higher content of G band carbon on 5Mn catalyst presented the higher crystalline degree of the carbon materials [44], which was also verified by XRD results. The reflection of carbon could be detected on spent 5Mn catalyst with the crystallite size of 12 nm (Table 5). It is observed that the 5Al catalyst exhibits the highest carbon deposition of 14.0 %, which is higher than the used 5Mn catalyst (6.3 %). While the crystallite size of carbon deposition on the used 5Al catalyst (11 nm) is smaller than on the used 5Mn catalyst (12 nm). A lot of carbon on 5Mn catalyst is the graphene

carbon, which is accordance with the Raman results. Therefore, the 5Al and 5Mn catalysts exhibited two kinds of carbon (disorder and graphite) with different ratio of $I_D/I_G$.

### 3.3 Basicity, physical-chemical features, and surface characterization

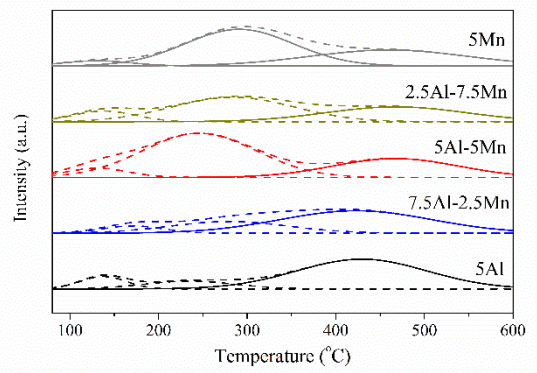


**Figure 4** The $CO_2$-TPD profiles of Ni-Zr-Al-Mn catalysts in situ reduction at 750 $^oC$

It is well known that basicity has a key role in the resistance against carbon formation in DRM since the carbon deposition derived from $CH_4$ decomposition is well-known to be deposited on the acid sites from the support [12]. Besides, the addition of basic promoters favors $CO_2$ adsorption and its dissociation, which contributes to the gasification of the carbon and thus to inhibiting the deactivation due to carbon formation [45-47]. Therefore, the lower concentration of basic sites might result in carbon deposition. $CO_2$-TPD was performed to evaluate the basicity of the studied catalysts; the results were presented in **Figure 4**. From $CO_2$-TPD plots, one can note that all Ni-Zr-Al-Mn catalysts present three typical $CO_2$ desorption peaks from 100 to 600 °C. First, one can note that the peaks in the $CO_2$-TPD curve on 5Mn, 2.5Al-7.5Mn, and 5Al-5Mn catalysts shift to low temperature compared to 7.5Al-2.5Mn and 5Al catalysts. This implies that the Mn promotion could lead to a decrease in the basicity of Ni-Zr-Al-Mn catalysts. Moreover, the total amount of basic sites varies differently. According to **Table 3**, the highest number of basic sites is obtained on the 5Al-5Mn catalyst (84 µmol $CO_2$/g), which is higher than Ni-Zr catalyst (73 µmol $CO_2$/g) [31]. The $CO_2$-TPD overall peak can be deconvoluted into three peaks corresponding to weak basic sites, medium-strength basic sites, and strong basic sites, which are mainly consisted

of weak Brønsted basic sites (surface OH groups), Lewis base sites (unsaturated (cus) $O^{2-}$ and $Zr^{4+}$–$O^{2-}$ centers), and the cus $Zr^{4+}$ centers with strong Lewis acidity, respectively [45, 48]. In this study, the highest content of medium-strength basic sites is obtained on the 5Al-5Mn catalyst (52 μmol $CO_2$/g). The ranking in $CO_2$ desorbed with medium-strength is as follows: 46 μmol $CO_2$/g for 5Mn > 43 μmol $CO_2$/g for Ni-Zr [31] > 33 μmol $CO_2$/g for 2.5Al-7.5Mn > 9 μmol $CO_2$/g for both 7.5Al-2.5Mn and 5Al catalysts. The introduction of Mn leads to a decrease in the amount of $CO_2$ corresponding to strong basic sites compared to Al-promoted catalysts. The medium-strength basic sites could promote the adsorption and/or activation of $CO_2$, and further reduce the carbon deposition, as well as the deactivation of catalyst as it had already been reported in the literature [2, 49, 50].

**Table 3** The $CO_2$-TPD profiles of Ni-Zr-Al-Mn catalysts in situ reduction at 750 °C

| | $CO_2$ desorbed (μmol $CO_2$ /g) | | | | | | |
|---|---|---|---|---|---|---|---|
| | Peak 1 weak | | Peak 2 medium-strength | | Peak 3 strong | | |
| Catalyst | Position (°C) | Content (%) | Position (°C) | Content (%) | Position (°C) | Content (%) | Total basicity (μmol $CO_2$/g) |
| 5Al | 134 | 7 | 231 | 9 | 435 | 47 | 63 |
| 7.5Al-2.5Mn | 169 | 4 | 282 | 9 | 425 | 44 | 57 |
| 5Al-5Mn | 129 | 8 | 248 | 52 | 469 | 24 | 84 |
| 2.5Al-7.5Mn | 136 | 9 | 281 | 33 | 467 | 22 | 64 |
| 5Mn | 133 | 7 | 288 | 46 | 474 | 24 | 77 |

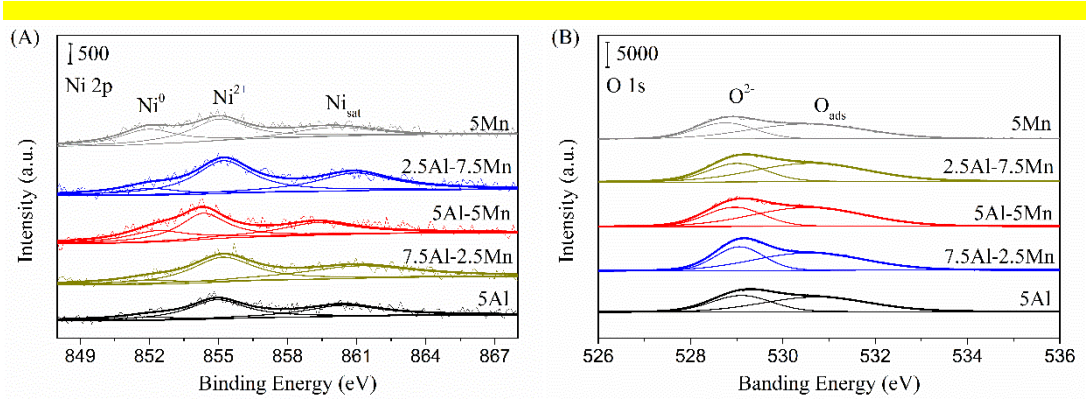

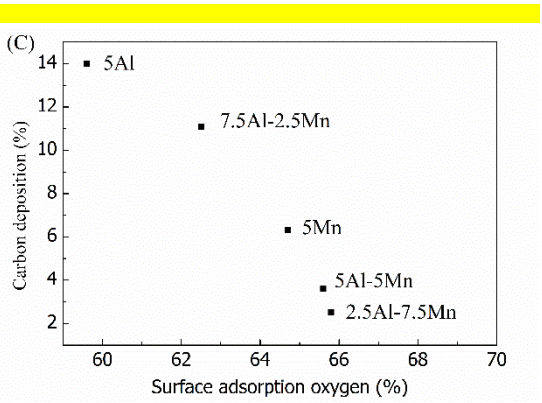


**Figure 5** (A) The Ni 2p and (B) the O 1s profiles of Ni-Zr-Al-Mn catalysts after reduction, and (C) the relationship between the carbon deposition and the content of surface adsorbed oxygen species.

**Table 4** presents the surface elemental content of reduced catalysts. The content of Ni species was 6.3, 6.8, 7.8, 8.9 and 8.6 % for 5Al, 7.5Al-2.5Mn, 5Al-5Mn, 2.5Al-7.5Mn, and 5Mn catalysts, respectively. It can be observed that the surface Ni content increased with the increase of Mn content when both Al and Mn promoters existed. It means the Mn enhance the enrichment of nickel species on the surface of catalyst. Besides, the Ni 2p curve (**Figure 5** (A)) was resolved to two peaks at about 852.3±0.5 eV, 854.5±0.5 eV with the corresponding satellite at about 861.0±0.5 eV, which were corresponded to $Ni^0$ and $Ni^{2+}$ species, respectively [51] (Figure 5). The content of each peak was listed in **Table 4**. The 5Al-5Mn catalyst showed the higher $Ni^0$ content than other Al-containing catalyst. The $Ni^0$ species might promote both the dry reforming of methane and methane decomposition [52]. Thus, the 5Mn-5Al catalyst exhibited higher activity for DRM reaction. Although the 5Mn catalyst exhibited the highest content of $Ni^0$ species of 3.6 %, it showed the lowest activity in the beginning, which might be caused by the methane decomposition, especially 5Mn catalyst that contained Ni in considerable amounts. The carbon deposition on 5Mn catalyst may cause its partial deactivation. Thus, the activity decreased within first one hour. Similar results have been reported in the literature [53].

**Table 4** The surface elemental content of 5Al, 7.5Al-2.5Mn, 5Al-5Mn, 2.5Al-7.5Mn, and 5Mn reduced catalysts.

| | Ni | Zr | Al | Mn | O |
|---|---|---|---|---|---|

| | Total (%) | $Ni^0$ (%) | $Ni^{2+}$ (%) | (%) | (%) | (%) | (%) |
|---|---|---|---|---|---|---|---|
| 5Al | 6.3 | 0.9 | 5.4 | 53.6 | 5.1 | - | 35.0 |
| 7.5Al-2.5Mn | 6.8 | 1.1 | 5.7 | 51.4 | 4.9 | 2.1 | 34.8 |
| 5Al-5Mn | 7.8 | 2.9 | 4.9 | 50.4 | 4.1 | 4.8 | 32.9 |
| 2.5Al-7.5Mn | 8.9 | 1.8 | 7.1 | 52.4 | 1.4 | 5.0 | 32.3 |
| 5Mn | 8.6 | 3.6 | 5 | 46.7 | - | 6.5 | 38.2 |

In addition to the basicity of the catalysts, one of the important factors is the adsorption of surface oxygen species, which is known to promote the activation of $CO_2$, leading to the decrease of the carbon deposition and the enhancement in the stability of the catalyst for DRM reaction [31, 54]. **Figure 5** (B) shows the O 1s profiles from XPS spectroscopy (526 to 536 eV) of reduced studied catalysts. The peak at about 529 eV is assigned to the lattice oxygen species ($O^{2-}$), while another peak at 531 eV is attributed to the adsorbed oxygen species ($O_{ads}$) [31, 54-56]. The highest content of surface adsorbed oxygen species is obtained on 2.5Al-7.5Mn catalyst (65.8 %), which also corresponds to the lowest carbon deposition, as shown in **Figure 5** (C). One can also note from Figure 5 (B) that the content of $O_{ads}$ species follows the sequence: 2.5Al-7.5Mn > 5Al-5Mn > 5Mn > 7.5Al-2.5Mn > 5Al. An opposite order in the carbon deposition can be observed on Ni-Zr-Al-Mn catalysts. This positive role of adsorbed oxygen species on $ZrO_2$ support has already been reported by Zhang et al. [54]. The author found the higher content of adsorbed oxygen species could contribute to the adsorption and activation of $CO_2$ and $CH_4$ dissociation in DRM. Herein, the carbon deposition decreases with the increase of the surface adsorbed oxygen species, confirming that the surface oxygen significantly improves resistance in the carbon deposition during DRM. On the other hand, the content of adsorbed oxygen species reflects the concentration of oxygen vacancies on catalyst [55]. Those oxygen vacancies could also promote the adsorption and activation of $CO_2$, which has already been reported in the literature [20, 24, 57]. Therefore, both aspects can contribute to the lower carbon deposition on the 5Al-5Mn and 2.5Al-7.5Mn catalysts.

The XRD patterns of calcined, reduced, and used Ni-Zr-Al-Mn catalysts are reported in **Figure 6**. The tetragonal $ZrO_2$ reflections with the crystallite sizes of 9 nm based on the Scherrer equation could be identified for all calcined, reduced, and used catalysts. The peak at about 43.3 ° and 44.5 °can be assigned to the NiO and $Ni^0$ species [58, 59]. The NiO reflections present on calcined catalysts, disappear on all the reduced catalysts, indicating that the nickel species have been reduced on all the reduced catalysts. As listed in **Table 5**, one can be noted that the existence of both Al and Mn results in a smaller crystalline size of nickel species (both NiO and $Ni^0$) on all catalysts. The same positive effect was observed for Al and Mn promoted catalysts in literature [60, 61]. The 2.5Al-7.5Mn and 5Al-5Mn catalysts have smaller crystallite sizes of $Ni^0$ species (<20 nm), which might contribute to their catalytic activity for DRM, because smaller size of nickel species would enhance the activity. Similar results have also been reported by He et al [33]. While it increases to 22, 20, and 27 nm on 5Al, 7.5Al-2.5Mn, and 5Mn catalysts, respectively. Those relatively large crystallite size of metallic nickel can lead to carbon deposition, thereby leading to lower selectivity for DRM and further resulting higher carbon deposition [5, 62, 63]. Especially on 5Al and 5Mn catalysts, the reflection of carbon could be detected on spent 5Al and 5Mn catalysts with the crystallite size of 11 and 12 nm, respectively. Besides, after 5 h DRM activity tests, slight sintering occurred on 2.5Al-7.5Mn catalyst after DRM tests, and the crystallite $Ni^0$ sizes increased from 16 nm to 18 nm. Thus, the activity of the 2.5Al-7.5Mn catalyst decreased a little with time on stream. While for others, the $Ni^0$ crystallite sizes of spent catalysts are slightly smaller than those on the reduced catalysts, since the redispersion of Ni species occurs upon continuous reduction and oxidation of nickel [5, 64]. which is in agreement with the results reported by Świrk [15].

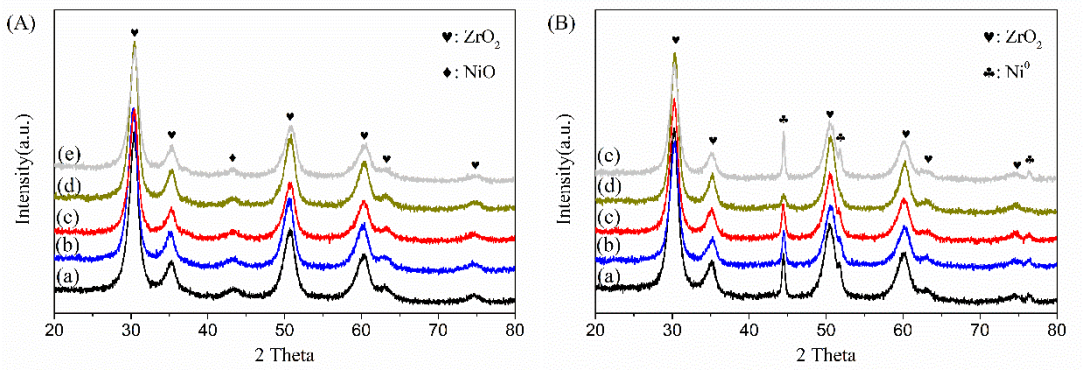

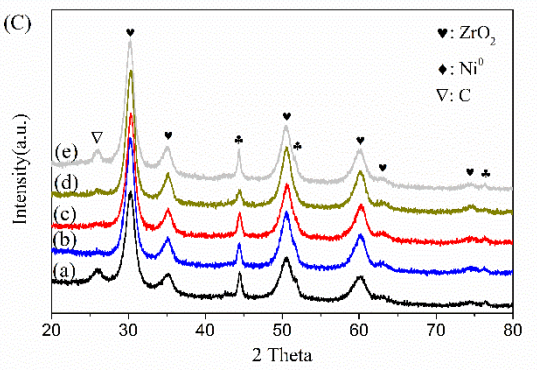


**Figure 6** The XRD results of (A) calcinated, (B) reduced and (C) used 5Al (a), 7.5Al-2.5Mn (b), 5Al-5Mn (c), 2.5Al-7.5Mn (d) and 5Mn (e) catalysts.

It implies that the other catalysts could suppress the sintering of nickel-metal during the DRM reaction. The $Ni^0$ crystallite sizes on 5Al, 7.5Al-2.5Mn, 5Al-5Mn and 5Mn catalysts decreased, while their activity showed different trend during the 5 h DRM. For 7.5Al-2.5Mn catalyst, the activity decreased. For the 5Al and 5Al-5Mn catalysts, the activity did not change. However, the activity on 5Mn catalyst decreased within one hour and then increased. The large particle size of $Ni^0$ on 5Mn catalyst resulted in carbon deposition, thereby led to partial deactivation. After reaction, the crystallite size of $Ni^0$ species decreased, while during the reaction process, the activity increased after one hour. Those phenomena mean the nickel redispersion might promote the activity for DRM by the existence of Mn. A similar phenomenon was reported by Li et al. [34].

**Table 5** Crystalline sizes of Ni-Zr-Al-Mn catalysts, after reduction at 750 °C for 1 hour and after reaction at 700 °C for 5 hours

| | $ZrO_2$ (nm) | | | NiO (nm) | $Ni^0$ (nm) | | C (nm) |
|---|---|---|---|---|---|---|---|
| | calcined | reduced | reaction | calcined | reduced | reaction | reaction |
| 5Al | 9 | 9 | 9 | 15 | 22 | 19 | 11 |
| 7.5Al-2.5Mn | 9 | 9 | 9 | 11 | 20 | 18 | - |
| 5Al-5Mn | 10 | 10 | 10 | 13 | 19 | 17 | - |
| 2.5Al-7.5Mn | 10 | 10 | 9 | 14 | 16 | 18 | - |
| 5Mn | 10 | 9 | 10 | 17 | 27 | 20 | 12 |

### 3.4 Discussion

It is well known that large nickel particle size may lead to carbon deposition [62, 63], and the low basic sites also affect the carbon deposition [19, 25]. For the 5Al-5Mn catalyst, both smaller nickel particle size and higher number of basic sites contribute to lower carbon deposition during DRM. More strong basic sites were formed on 5Al and 7.5Al-2.5Mn catalysts, resulting in a higher carbon deposition since strong basic sites would lead to too strong adsorption of $CO_2$. Similar results were reported in the literature [49]. Besides, the weak and medium-strength basic sites could promote the adsorption and/or activation of $CO_2$, and further reduce the carbon deposition [2, 49, 50]. It has been also found that the addition of Mn promoter leads to a reduction not only of the formation of coke but also in the rate of the DRM reaction [28, 60, 65], therefore, the 5Mn catalyst exhibited slight lower carbon deposition (lower than 5Al) and lower activity for DRM in the beginning. Besides, the adsorbed oxygen species is inversely proportional to carbon deposition. Higher content of adsorbed oxygen species results in lower carbon deposition. Because adsorbed oxygen species contribute to the adsorption and activation of $CO_2$, thereby reducing the carbon deposition [31, 54].

## 4. Conclusions

Al and Mn-promoted Ni catalysts supported on $ZrO_2$ were synthesized by a one-step synthesis method and tested in DRM at 700 °C with the GSHV of 48,000 $h^{-1}$. Based on the DRM results, the addition of both Al and Mn promoters could enhance the activity with lower carbon deposition for dry reforming of methane. And the 5Al-5Mn (5 wt% Al and 5 wt% Mn) catalyst exhibited the highest catalytic performance for DRM, as well as the lower carbon deposition. According to the XRD, XPS, and $CO_2$-TPD characterizations, the results showed more medium-strength basic sites, smaller crystallite size, and higher content of adsorbed oxygen species on the 5Al-5Mn catalyst. All the properties were beneficial for catalyst stability in limiting the carbon deposition. Meanwhile, this work clearly showed that the adsorbed oxygen species was inversely related to carbon deposition. That is the more adsorbed oxygen species, the less carbon deposition.

## CRediT authorship contribution statement

Ye: Conceptualization, Investigation, Formal analysis, Writing - original draft, Writing - review &

editing. Li: Investigation, Writing - review & editing. Cui: Investigation, Writing - review & editing. Patrick: Conceptualization, Supervision, Writing - review & editing. Changwei: Conceptualization, Supervision, Writing - review & editing.

**Acknowledgments**

Ye Wang acknowledges the financial support of CSC (China Scholarship Council) for her joint-PhD research at Sorbonne Université. We thank Yunfei Tian of the analytical & testing center of Sichuan University for XPS experiments.

**Funding**

This work was supported by the National Key R&D Program of China (2018YFB1501404), the 111 program (B17030), and Fundamental Research Funds for the Central Universities.

**Notes**

The authors declare no competing financial interest.

**References**

[1] S. Corthals, J. V. Nederkassel, H. D.Winne, Design of active and stable $NiCeO_2ZrO_2MgAl_2O_4$ dry reforming catalysts, Appl. Catal. B: Environ. 105 (2011) 263-275.

[2] Y. Wang, L. Yao, S. Wang, D. Mao, C. Hu, Low-temperature catalytic $CO_2$ dry reforming of methane on Ni-based catalysts: a review, Fuel Process. Technol. 169 (2018) 199-206.

[3] E. Ryckebosch, M. Drouillon, H. Vervaeren, Techniques for transformation of biogas to biomethane, Biomass Bioenerg. 35 (2011) 1633-1645.

[4] A. Djaidja, S. Libs, A. Kiennemann, A. Barama, Characterization and activity in dry reforming of methane on NiMg/Al and Ni/MgO catalysts, Catal. Today, 113 (2006) 194-200.

[5] Y. Wang, L. Li, Y. Wang, P. Da Costa, C. Hu, Highly Carbon-Resistant Y Doped $NiO–ZrO_m$ Catalysts for Dry Reforming of Methane, Catalysts, 9 (2019) 1055.

[6] C. Wang, N. Sun, N. Zhao, W. Wei, Y. Zhao, Template-free preparation of bimetallic mesoporous Ni-Co-CaO-$ZrO_2$ catalysts and their synergetic effect in dry reforming of methane, Catal. Today, 281 (2017) 268-275.

[7] J. Titus, T. Roussiere, G. Wasserschaff, S. Schunk, A. Milanov, E. Schwab, G. Wagner, O. Oeckler, R. Gläser, Dry reforming of methane with carbon dioxide over NiO–MgO–$ZrO_2$, Catal. Today, 270 (2016) 68-75.

[8] A. Ochoa, A. Arregi, M. Amutio, A.G. Gayubo, M. Olazar, J. Bilbao, P. Castaño, Coking and sintering progress of a Ni supported catalyst in the steam reforming of biomass pyrolysis volatiles, Appl. Catal. B: Environ. 233 (2018) 289-300.

[9] Q. Zhang, T. Zhang, Y. Shi, B. Zhao, M. Wang, Q. Liu, J. Wang, K. Long, Y. Duan, P. Ning, A sintering and carbon-resistant Ni-SBA-15 catalyst prepared by solid-state grinding method for dry reforming of methane, J. $CO_2$ Util. 17 (2017) 10-19.

[10] Y. Lou, M. Steib, Q. Zhang, K. Tiefenbacher, A. Horváth, A. Jentys, Y. Liu, J.A. Lercher, Design of stable Ni/$ZrO_2$ catalysts for dry reforming of methane, J. Catal. 356 (2017) 147-156.

[11] Q. Chen, J. Zhang, B. Pan, W. Kong, Y. Chen, W. Zhang, Y. Sun, Temperature-dependent anti-coking behaviors of highly stable Ni-CaO-$ZrO_2$ nanocomposite catalysts for $CO_2$ reforming of methane, Chem. Eng. J. 320 (2017) 63-73.

[12] J. Won-Jun, S. Jae-Oh, K. Hak-Min, Y. Seong-Yeun, R. Hyun-Seog, A review on dry reforming of methane in aspect of catalytic properties, Catal. Today, 324 (2019) 15-26.

[13] K. Mette, S. Kühl, A. Tarasov, H. Düdder, K. Kähler, M. Muhler, R. Schlögl, M. Behrens, Redox dynamics of Ni catalysts in $CO_2$ reforming of methane, Catal. Today, 242 (2015) 101-110.

[14] L.A. Arkatova, The deposition of coke during carbon dioxide reforming of methane over intermetallides, Catal. Today, 157 (2010) 170-176.

[15] K. Świrk, M.E. Galvez, M. Motak, T. Grzybek, M. Rønning, P. Da Costa, Dry reforming of methane over Zr-and Y-modified Ni/Mg/Al double-layered hydroxides, Catal. Commun. 117 (2018) 26-32.

[16] M. Miyamoto, A. Hamajima, Y. Oumi, S. Uemiya, Effect of basicity of metal doped $ZrO_2$ supports on hydrogen production reactions, Int. J. Hydrogen Energ. 43 (2018) 730-738.

[17] S.M. Sajjadi, M. Haghighi, F. Rahmani, Sol–gel synthesis of Ni–Co/$Al_2O_3$–MgO–$ZrO_2$ nanocatalyst used in hydrogen production via reforming of $CH_4$/$CO_2$ greenhouse gases, J. Nat. Gas Sci. Eng. 22 (2015) 9-21.

[18] L. Yao, J. Shi, H. Xu, W. Shen, C. Hu, Low-temperature $CO_2$ reforming of methane on Zr-promoted Ni/$SiO_2$ catalyst, Fuel Process. Technol. 144 (2016) 1-7.

[19] X. Zhao, Y. Cao, H. Li, J. Zhang, L. Shi, D. Zhang, Sc promoted and aerogel confined Ni catalysts for coking-resistant dry reforming of methane, RSC Adv. 7 (2017) 4735-4745.

[20] Y.J. Asencios, C.B. Rodella, E.M. Assaf, Oxidative reforming of model biogas over NiO–$Y_2O_3$–$ZrO_2$ catalysts, Appl. Catal. B: Environ. 132 (2013) 1-12.

[21] B. Koubaissy, A. Pietraszek, A. Roger, A. Kiennemann, $CO_2$ reforming of methane over Ce-Zr-Ni-Me mixed catalysts, Catal. Today, 157 (2010) 436-439.

[22] F. Pompeo, N.N. Nichio, O.A. Ferretti, D. Resasco, Study of Ni catalysts on different supports to obtain synthesis gas, Int. J. Hydrogen Energ. 30 (2005) 1399-1405.

[23] N. Wang, W. Chu, T. Zhang, X.-S. Zhao, Manganese promoting effects on the Co–Ce–Zr–$O_x$ nano catalysts for methane dry reforming with carbon dioxide to hydrogen and carbon monoxide, Chem. Eng. J. 170 (2011) 457-463.

[24] J.D. Bellido, E.M. Assaf, Effect of the $Y_2O_3$–$ZrO_2$ support composition on nickel catalyst evaluated in dry reforming of methane, Appl. Catal. A: Gen. 352 (2009) 179-187.

[25] H. Liu, H.B. Hadjltaief, M. Benzina, M.E. Gálvez, P. Da Costa, Natural clay based nickel catalysts for dry reforming of methane: On the effect of support promotion (La, Al, Mn), Int. J. Hydrogen Energ. 44 (2019) 246-255.

[26] S.K. Talkhoncheh, M. Haghighi, Syngas production via dry reforming of methane over Ni-based nanocatalyst over various supports of clinoptilolite, ceria and alumina, J. Nat. Gas Sci. Eng. 23 (2015) 16-25.

[27] A.E.C. Luna, M.E. Iriarte, Carbon dioxide reforming of methane over a metal modified Ni-$Al_2O_3$ catalyst, Appl. Catal. A: Gen. 343 (2008) 10-15.

[28] Y. Lu, J. Zhu, X. Peng, D. Tong, C. Hu, Comparative study on the promotion effect of Mn and Zr on the stability of Ni/$SiO_2$ catalyst for $CO_2$ reforming of methane, Int. J. Hydrogen Energ. 38 (2013) 7268-7279.

[29] S.-H. Seok, S.H. Choi, E.D. Park, S.H. Han, J.S. Lee, Mn-promoted Ni/$Al_2O_3$ catalysts for stable carbon dioxide reforming of methane, J. Catal. 209 (2002) 6-15.

[30] C. Li, P.-J. Tan, X.-D. Li, Y.-L. Du, Z.-H. Gao, W. Huang, Effect of the addition of Ce and Zr on the structure and performances of Ni–Mo/CeZr–MgAl(O) catalysts for $CH_4$–$CO_2$ reforming, Fuel Process. Technol. 140 (2015) 39-45.

[31] Y. Wang, Q. Zhao, Y. Wang, C. Hu, P. Da Costa, One-step synthesis of highly active and

stable Ni-$ZrO_x$ for dry reforming of methane, Ind. Eng. Chem. Res. 59 (2020) 11441–11452.

[32] W. Li, X. Jie, C. Wang, J.R. Dilworth, C. Xu, T. Xiao, P.P. Edwards, $MnO_x$-Promoted, Coking-Resistant Nickel-based Catalysts for Microwave-initiated $CO_2$ Utilization, Ind. Eng. Chem. Res. 59 (2020) 6914–6923

[33] S. He, H. Wu, W. Yu, L. Mo, H. Lou, X. Zheng, Combination of $CO_2$ reforming and partial oxidation of methane to produce syngas over Ni/$SiO_2$ and Ni–$Al_2O_3$/$SiO_2$ catalysts with different precursors, Int. J. Hydrogen Energ. 34 (2009) 839-843.

[34] X. Li, J.S. Chang, M. Tian, S.E. Park, $CO_2$ reforming of methane over modified Ni/$ZrO_2$ catalysts, Appl. Organomet. Chem. 15 (2001) 109-112.

[35] Y. Wang, L. Yao, Y. Wang, S. Wang, Q. Zhao, D. Mao, C. Hu, Low-temperature catalytic $CO_2$ dry reforming of methane on Ni-Si/$ZrO_2$ catalyst, ACS Catal. 8 (2018) 6495-6506.

[36] M.K. Nikoo, N. Amin, Thermodynamic analysis of carbon dioxide reforming of methane in view of solid carbon formation, Fuel Process. Technol. 92 (2011) 678-691.

[37] M.M. Souza, D.A. Aranda, M. Schmal, Reforming of methane with carbon dioxide over Pt/$ZrO_2$/$Al_2O_3$ catalysts, J. Catal. 204 (2001) 498-511.

[38] J. Rostrupnielsen, J.B. Hansen, $CO_2$-reforming of methane over transition metals, J. Catal. 144 (1993) 38-49.

[39] Ş. Özkara-Aydınoğlu, A.E. Aksoylu, Carbon dioxide reforming of methane over Co-X/$ZrO_2$ catalysts (X= La, Ce, Mn, Mg, K), Catal. Commun. 11 (2010) 1165-1170.

[40] K. Świrk, M.E. Galvez, M. Motak, T. Grzybek, M. Rønning, P. Da Costa, Yttrium promoted Ni-based double-layered hydroxides for dry methane reforming, J. $CO_2$ Util. 27 (2018) 247-258.

[41] T. Bai, X. Zhang, F. Wang, W. Qu, X. Liu, C. Duan, Coking behaviors and kinetics on HZSM-5/SAPO-34 catalysts for conversion of ethanol to propylene, J. Energ. Chem. 25 (2016) 545-552.

[42] A.R. McFarlane, I.P. Silverwood, E.L. Norris, R.M. Ormerod, C.D. Frost, S.F. Parker, D. Lennon, The application of inelastic neutron scattering to investigate the steam reforming of methane over an alumina-supported nickel catalyst, Chem. Phys. 427 (2013) 54-60.

[43] A. Sadezky, H. Muckenhuber, H. Grothe, R. Niessner, U. Pöschl, Raman microspectroscopy of soot and related carbonaceous materials: Spectral analysis and structural information, Carbon, 43 (2005) 1731-1742. 22 (2015) 9-21

[44] S.A. Chernyak, A.S. Ivanov, K.I. Maslakov, A.V. Egorov, Z. Shen, S.S. Savilov, V.V. Lunin, Oxidation, defunctionalization and catalyst life cycle of carbon nanotubes: a Raman spectroscopy view, Phys. Chem. Chem. Phys. 19 (2017) 2276.

[45] H. Liu, D. Wierzbicki, R. Debek, M. Motak, T. Grzybek, P.D. Costa, M.E. Gálvez, La-promoted Ni-hydrotalcite-derived catalysts for dry reforming of methane at low temperatures, Fuel, 182 (2016) 8-16.

[46] R. Dębek, M.E. Galvez, F. Launay, M. Motak, T. Grzybek, P. Da Costa, Low temperature dry methane reforming over Ce, Zr and CeZr promoted Ni–Mg–Al hydrotalcite-derived catalysts, Int. J. Hydrogen Energ. 41 (2016) 11616-11623.

[47] V. García, J.J. Fernández, W. Ruíz, F. Mondragón, A. Moreno, Effect of MgO addition on the basicity of Ni/$ZrO_2$ and on its catalytic activity in carbon dioxide reforming of methane, Catal. Commun. 11 (2009) 240-246.

[48] X. Zhang, Q. Zhang, N. Tsubaki, Y. Tan, Y. Han, Carbon dioxide reforming of methane over Ni nanoparticles incorporated into mesoporous amorphous $ZrO_2$ matrix, Fuel, 147 (2015) 243-252.

[49] R. Dębek, M. Motak, M.E. Galvez, T. Grzybek, P. Da Costa, Influence of Ce/Zr molar ratio on catalytic performance of hydrotalcite-derived catalysts at low temperature $CO_2$ methane reforming, Int. J. Hydrogen Energ. 42 (2017) 23556-23567.

[50] R. Dębek, M. Motak, M.E. Galvez, P. Da Costa, T. Grzybek, Catalytic activity of hydrotalcite-derived catalysts in the dry reforming of methane: on the effect of Ce promotion and feed gas composition, React. Kinet. Mech. Cat. 121 (2017) 185-208.

[51] Y. Xu, H. Long, Q. Wei, X. Zhang, S. Shang, X. Dai, Y. Yin, Study of stability of Ni/MgO/γ-$Al_2O_3$ catalyst prepared by plasma for $CO_2$ reforming of $CH_4$, Catal. Today, 211 (2013) 114–119.

[52] A. F. Al-Fastesh, R. Kumar, S. O. Kasim, A .A .Ibrahim, A. H. Fakeeha, A. E. Abasaeed, R. Alrasheed, A. Bagabas, M. L. Chaudary, F. Frusteri, B. Chowdhury, The effect of modifier identity on the performance of Ni-based catalyst supported on γ-$Al_2O_3$ in dry reforming of methane, Catal. Today, 348 (2020) 236-242.

[53] R. Dębek, M. Motak, D. Duraczyska, F. Launay, M.E. Galvez, T. Grzybek, P. Da Costa, Methane dry reforming over hydrotalcite-derived Ni–Mg–Al mixed oxides: the influence of Ni

content on catalytic activity, selectivity and stability, Catal. Sci. Technol. 6 (2016) 6705-6715.

[54] M. Zhang, J. Zhang, Y. Wu, J. Pan, Q. Zhang, Y. Tan, Y. Han, Insight into the effects of the oxygen species over Ni/$ZrO_2$ catalyst surface on methane reforming with carbon dioxide, Appl. Catal. B: Environ. 244 (2019) 427-437.

[55] H. Wang, J. Liu, Z. Zhao, Y. Wei, C. Xu, Comparative study of nanometric Co-, Mn- and Fe-based perovskite-type complex oxide catalysts for the simultaneous elimination of soot and $NO_x$ from diesel engine exhaust, Catal. Today, 184 (2012) 288-300.

[56] H. Liang, Y. Hong, C. Zhu, S. Li, Y. Chen, Z. Liu, D. Ye, Influence of partial Mn-substitution on surface oxygen species of $LaCoO_3$ catalysts, Catal. Today, 201 (2013) 98-102.

[57] Y.J.O. Asencios, F.C.F. Marcos, J.M. Assaf, E.M. Assaf, Oxidative-reforming of methane and partial oxidation of methane reaction over NiO/$PrO_2$/$ZrO_2$ catalysts: effect of the nickel content, Braz. J. Chem. Eng. 33 (2016) 627-636.

[58] L. Yao, Y. Wang, J. Shi, H. Xu, W. Shen, C. Hu, The influence of reduction temperature on the performance of $ZrO_x$/Ni-$MnO_x$/$SiO_2$ catalyst for low-temperature $CO_2$ reforming of methane, Catal. Today, 281 (2017) 259-267.

[59] Z. Miao, Z. Li, C. Suo, J. Zhao, W. Si, J. Zhou, S. Zhuo, One-pot synthesis of $Al_2O_3$ modified mesoporous $ZrO_2$ with excellent thermal stability and controllable crystalline phase, Adv. Powder Technol. 29 (2018) 3569-3576.

[60] F. Guo, J.-Q. Xu, W. Chu, $CO_2$ reforming of methane over Mn promoted Ni/$Al_2O_3$ catalyst treated by $N_2$ glow discharge plasma, Catal. Today, 256 (2015) 124-129.

[61] X. Liu, J. Toyir, P. Ramirez de la Piscina, N. Homs, Hydrogen production from methanol steam reforming over $Al_2O_3$- and $ZrO_2$-modified CuOZnO$Ga_2O_3$ catalysts, Int. J. Hydrogen Energ. 42 (2017) 13704-13711.

[62] K. Świrk, M.E. Gálvez, M. Motak, T. Grzybek, M. Rønning, P. Da Costa, Syngas production from dry methane reforming over yttrium-promoted nickel-KIT-6 catalysts, Int. J. Hydrogen Energ. 44 (2019) 274-286.

[63] K. Sutthiumporn, S. Kawi, Promotional effect of alkaline earth over Ni–$La_2O_3$ catalyst for $CO_2$ reforming of $CH_4$: role of surface oxygen species on $H_2$ production and carbon suppression, Int. J. Hydrogen Energ. 36 (2011) 14435-14446.

[64] T. Nakayama, M. Arai, Y. Nishiyama, Dispersion of nickel particles supported on alumina

and silica in oxygen and hydrogen, J. Catal. 87 (1984) 108-115.

[65] T. Osaki, T. Mori, Role of potassium in carbon-free $CO_2$ reforming of methane on K-promoted $Ni/Al_2O_3$ catalysts, J. Catal. 204 (2001) 89-97